IIETA International Information and Engineering Technology Association
Advancing the World of Information and Engineering

Mathematical Modelling of Engineering Problems
Vol. 11, No. 11, November, 2024, pp. 2967-2976
Journal homepage: http://iieta.org/journals/mmep

Numerical Simulation of Waves Propagated from Driven Piles to Nearby Structures in Basra Soil

Hamed S. Saher[1*], Jaafar K. Ali[2], Haider S. Al-Jubair[1]

[1] Department of Civil Engineering, College of Engineering, University of Basrah, Basrah 61004, Iraq
[2] Department of Mechanical Engineering, College of Engineering, University of Basrah, Basrah 61004, Iraq

Corresponding Author Email: hamidsalim26@gmail.com

https://doi.org/10.18280/mmep.111109

Received: 15 January 2024
Revised: 17 March 2024
Accepted: 25 March 2024
Available online: 29 November 2024

Keywords:
driven piles, Plaxis 3D, numerical simulation, Basra, safe distance, peak particle velocity

ABSTRACT

The waves induced due to pile driving are investigated numerically, using the finite element method utilizing Plaxis-3D. Three locations are selected in Basra governorate-Iraq (Al-Fao, Shuaiba, and Umm Qasr), with various soil profiles, and different pile and hammer types to conduct the study. The predicted response in each site is compared to real measurements conducted (previously) by the authors. The regression analyses indicate excellent agreement between the predicted and measured variations of peak particle velocities with distance for various pile penetrations. It is proved that; the waveform of the impact hammer is a necessary input for a good simulation. The possible effects of pile driving operations on the environment, especially ground vibrations, are better understood according to this study. To reduce the negative influence on the local environment and buildings, it is essential to have this information to do comprehensive environmental impact assessments before building projects. It is realized that pile driving in soft soil deposits has negligible effects on shallow foundations of the nearby structures. For other profiles, the safe distance between the driven pile and an ordinary residential building is about (18) times the pile section's least dimension. This study contributes to our knowledge of pile-driving effects in various soil profiles, which in turn improves our capacity to simulate these effects, provides site-specific suggestions, and provides practical instructions for making construction projects safer and more sustainable.

1. INTRODUCTION

When the hammer strikes the pile, energy transfers into the pile and causes pile penetration. Some energy is lost through shear at the pile shaft and compression at the pile tip (Figure 1). Energy transfers away from the pile as traveling stress waves into the ground. This energy depends on the vibrating source and the medium that vibration transfers through it. It directly affects the surrounding vibration receivers such as human beings, equipment, structures, or anything sensitive to vibration [1].

Neglecting energy losses, the velocity of the dropping hammer is calculated as in reference [2]:

$$V_{H0} = (2\ g\ h)^{0.5} \quad (1)$$

where, V_{H0}: velocity of the hammer (m/s); g: acceleration due to gravity (m/s^2); h: height of drop (m).

The velocity of the pile head increases while the velocity of the hammer decreases due to pile impedance, as explained in Eq. (2) [3]:

$$Z_H * V_H = Z_P * V_P \quad (2)$$

where, $Z_{H,P}$: hammer and pile impedance (kN.s/m), respectively; $V_{H,P}$: hammer and pile particle velocity (m/s), respectively.

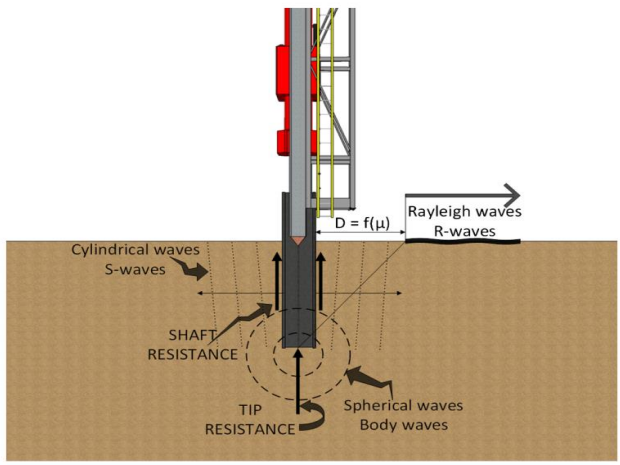

Figure 1. Vibration transmission mechanisms between pile and soil

The time (t) required to propagate the wave from the pile head towards the pile toe and reflect to the pile head again could be calculated as:

$$t = 2L_p/C_p \quad (3)$$

where, L_p: pile length (m); C_p: velocity of wave in the pile (m/s).

Many research articles have been published regarding the utilization of the finite element method in simulating the problem of vibrations induced due to pile driving. A streamlined axisymmetric model was established by Zhang et al. [4] to replicate the pile driving procedure utilizing Plaxis-2D software. The 15-noded element was selected to represent both the pile and the soil, while their connection was simulated using interface elements. Additionally, a simplified structure, comprised of beam elements, was positioned at a distance where ground vibrations were monitored. The finite element analyses yielded outcomes related to ground vibrations near the building and the building's reactions to the dynamic pile load. Afterward, comparisons were made regarding the structural responses, examining normal and shear stresses against their respective strengths. Andersson Olivecrona and Sulander [5] explored the potential for creating an effective finite element simulation of pile-driving-induced vibrations. The study delves into analyzing and contrasting the vibrations resulting from a single hammer impact at various depths of the pile, juxtaposed with real-world field test data. The successful application of the finite element method enabled accurate prediction of wave propagation and vibrations resulting from impact pile driving. The results indicated that the behavior and intensity of vibrations are significantly influenced by Young's modulus of the soil. Grizi et al. [6] investigated the ground vibration produced by driving a (1.7 m) H-Pile into a small-scale model of sandy soil. The findings indicated a strong alignment between the numerical outcomes and the observed data. Furthermore, there was a swift decrease in the peak particle velocity (PPV) as the distance from the pile increased. When the pile's tip went beyond a depth of (0.5 m), the numerical results underestimated the measured response. Sun et al. [7] utilized ABAQUS software to study the vibration effects on a nearby pre-existing pile, caused by a (1.25 m) diameter and (52.1 m) long new pile driving. The distance between the driven and existing piles varied between (10) times to (150) times the driven pile diameter. The lateral and vertical peak accelerations at the preexisting pile were found to be close to those in the free field. Additionally, within (20) diameters and greater distances, the acceleration at the existing pile diminished consistently as the distance increased.

Vibrations have a direct effect on the surrounding structures, three kinds of problems are induced by pile driving [2]:

(1) Vibration receivers may be human beings or anything sensitive to vibration.

(2) Medium that vibration can transfer through it.

(3) Vibration source.

To guarantee the safety, environmental sustainability, and regulatory compliance of building projects, it is crucial to study the impacts of pile-driving vibrations on nearby buildings, and a knowledge of how these vibrations affect structural integrity. To facilitate sustainable building methods, it is crucial to analyze the environmental effects to undertake thorough environmental impact assessments. Engineers can adapt techniques and tools to unique situations thanks to this information, which is included in building planning and design. The development of effective mitigation solutions, such as changes to building practices and the use of dampening devices, may be facilitated by recognizing possible consequences. Construction projects are more financially viable when they address neighborhood concerns about noise and vibrations. Researching the consequences of pile-driving vibrations helps with responsible construction methods, better decision-making, and more acceptability and success for building projects as a whole.

The research objective is to achieve successful numerical modeling of the problem of pile driving induced vibrations into Basrah soil utilizing the finite element method, and using this model in assessing the safe distance of a hypothetical structure based on AASHTO standards. This study helps us understand and simulate the consequences of pile driving, gives us ideas for particular sites, and gives us practical guidance to make construction sites safer. Three sites are selected to conduct the study, namely Al-Fao, Al-Shuaiba, and Umm Qasr, as shown in Figure 2.

Figure 2. Locations of the case studies

2. METHODOLOGY AND MATERIALS

2.1 Description

As a first step before starting the analysis by Plaxis-3D, verification should be conducted to check the validation of the program and give accurate results. A detailed verification for the steel pile 162 mm diameter [8] is attached in Appendix A, the matching ratio was 93.4 which means validation underscores the suitability of Plaxis-3D for evaluating dynamic load-induced vibrations, as it demonstrates very strong concordance with measured vibration data.

The first case study is a (1.22 m) outer diameter, (25 mm) thick, and (50 m) long tubular steel pile embedded in the Al-Fao site by using an S280 Hydro hammer. The second is a (0.4 m×0.4 m×10.5 m) precast reinforced concrete pile embedded in the Al-Shuaiba site by using an MAIT hammer, and the third one is a (0.4 m×0.4 m×12 m) precast reinforced concrete pile penetrating Umm Qasr site by using Junttan hammer.

The measured parameters collected from the sites represented by the peak particle velocity (PPV) by geophones,

waveform, and energy by using the Pile Dynamic Analyzer (PDA).

The availability of projects involving pile driving with various types of heaps and hammers led to the selection of these sites. These locations also served as examples of various soil profiles, which gave insight into how soil quality affected vibration-induced vibration.

2.2 Governing equation

The expression representing the discretized equation describing the motion of a volume subjected to a dynamic load over time is formulated as follows [9]:

$$[M]\{\ddot{d}\} + [C]\{\dot{d}\} + [K]\{d\} = \{F\} \quad (4)$$

where, $[M]$: Element mass matrix; $\{\ddot{d}\}$: Acceleration vector; $[C]$: Damping matrix; $\{\dot{d}\}$: Velocity vector; $[K]$: Element stiffness matrix; $\{d\}$: Displacement vector; $\{F\}$: Load vector.

The response at any time is predicted by integrating the above equation concerning the time.

2.3 Material characteristics

Soil characteristics, as obtained from the site investigation programs [10-12] and calculated using correlative relations, are listed in Tables 1-3. The constitutive relations used in Plaxis-3D simulation are also mentioned (Mohr-Coulomb [MC] or Hardening Soil [HS] model with small strain stiffness or Soft Soil model [SS]).

Pile and hammer characteristics used in each site are listed in Tables 4 and 5, respectively. It should be mentioned that the piles are modeled as elastic materials.

Table 1. Soil characteristics of Al-Fao site

No.	Depth (m)	Description	SPT	γt kN/m^3	Vs m/s	E kPa	ν	Fnmax	Model
Fill	0-2	Sand	10	19	157.7	15930	0.25	19.7	MC
A	2-25	Silty Clay	2	19	58	10000	0.3	0.63	SS
B	25-29.5	Silty Sand	4	19	99.6	36060	0.3	5.53	MC
C, D	29.5-50	Dense Sand	50	20	266.7	54100	0.25	3.33	MC

Table 2. Soil characteristics of the Al-Shuaiba site

No.	Depth (m)	Description	SPT	γt kN/m^3	Vs m/s	E kPa	ν	Fnmax	Model
L1	0–0.5	Silty Sand	2	18.4	76	10200	0.26	38	MC
L2	0.5-2	Stiff Clay	17	19.8	175.11	19200	0.3	29.185	HS
L3	2-5	Clay	5	19.1	108.65	12000	0.3	9.05	HS
L4	5-9	Sandy Clay	8	19.4	130.51	13800	0.28	8.16	HS
L5	9-11	Silty Clay	47	20.5	260.34	37200	0.29	32.54	HS

Table 3. Soil characteristics of the umm Qaser site

No.	Depth (m)	Description	SPT	γt kN/m^3	Vs m/s	E kPa	ν	Fnmax	Model
L1	0-2.75	Silty Sand	42	18.5	249.169	34200	0.27	22.65	MC
L2	2.75-7.25	Sandy Silt	50	19.5	266.7	39000	0.25	14.82	HS
L3	7.25-14	Silty Sand	43	19.5	251.47	34800	0.27	9.31	MC

Table 4. Pile characteristics

Site	Section (m)	f'c (MPa)	E (MPa)	Length (m)	F_y (MPa)	Wave Speed (m/s)	Z_p (kN/m)
Al-Fao	1.22 dia.	-	2.1×10^5	50	460	5263	3789
Shuaiba	0.4x 0.4	43.75	39200	10.5	460	4000	1568
Umm Qasr	0.4x0.4	45	40100	12	460	4050	1584

Table 5. Hammer characteristics

Site	Drop Height (m)	Weight of Ram (kg)	Energy (KJ)	Blows per Minute	Total Weight (kg)	Drive Cap Size (m)
Al-Fao	-	14000	280	45	31000	-
Shuaiba	1.2	9000	108	30 - 60	14500	0.55x0.55
Umm Qasr	0.9	6000	54	40 - 100	9700	0.55x0.55

2.4 Discretized models

The adopted model sizes are (100 m×100 m×50 m) for the first case study and (50 m×50 m×13 m) for the others. Ten-node tetrahedral volume elements are used to model the soil strata for all sites. Medium mesh distribution is used with a refinement activated for the pile and the region in the vicinity of the pile (Figure 3).

Plate elements are used to model the tubular steel pile to adopt the complex interactions between in-plane and out-of-plane deformations that occur in thin structures subjected to various loading conditions, whereas embedded beam elements are adopted to model the precast reinforced concrete piles by using the 2,3,5-nodes element is employed to represent lines or beams element. Depending on upon number of nodes in the element the shape function will be (first, second, fourth) ordered accordingly (Figure 4).

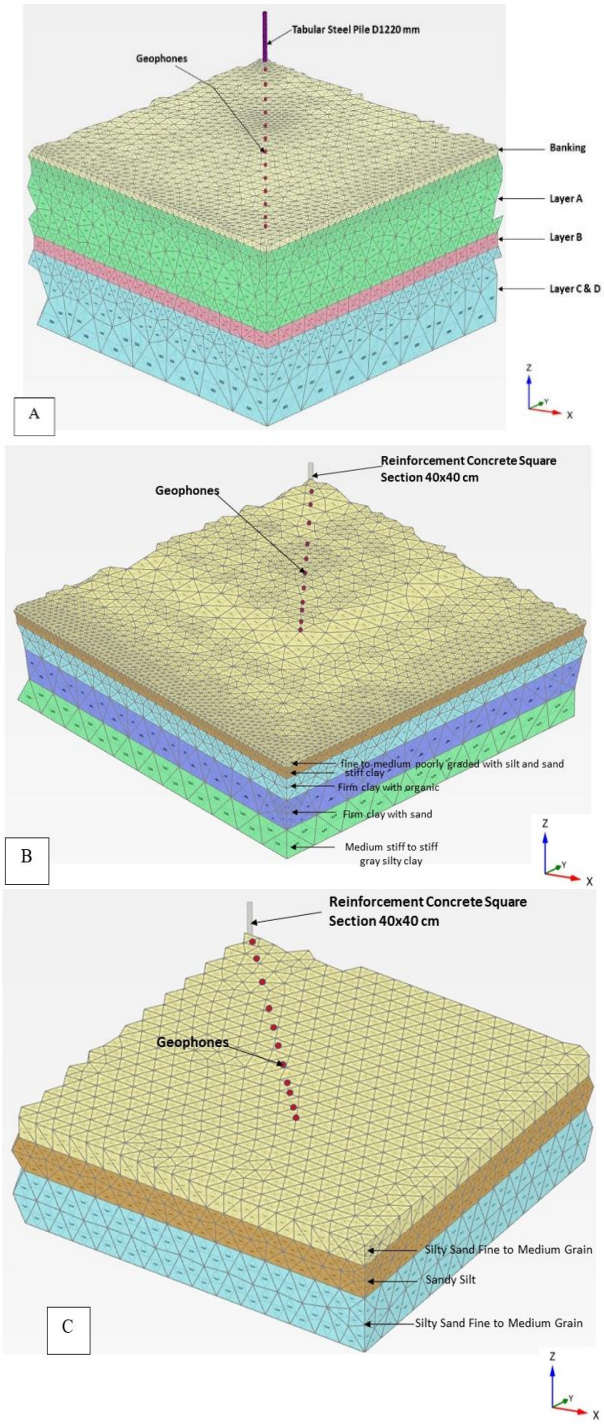

Figure 3. Discretization of soil mass of: (A) Al-Fao site; (B) Shuaiba site; (C) Umm qasr site

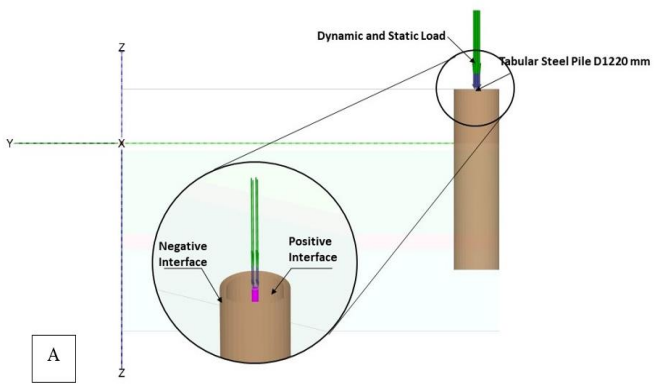

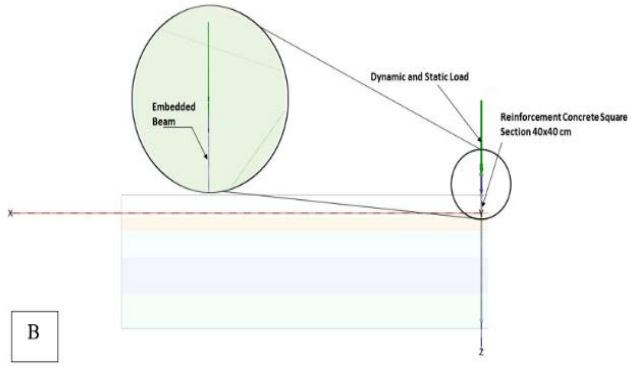

Figure 4. Piles modelling of (A) Al-Fao site; (B) Shuaiba and umm qasr sites

2.5 Boundary conditions

The boundary conditions are listed in Table 6.

Table 6. Boundary conditions of the deformation and dynamic analyses

Boundary	Deformation Analysis	Dynamic Analysis
Minimum X	Normally Fixed	None
Maximum X	Normally Fixed	Viscous
Minimum Y	Normally Fixed	None
Maximum Y	Normally Fixed	Viscous
Minimum Z	Fully Fixed	Viscous
Maximum Z	Free	None

2.6 Interfaces

Interfaces serve as connecting components intended for incorporation into plates or geogrids, enabling an accurate representation of soil-structure interplay within modelling. According to Table 7, the mode (from the adjacent soil) assigned for a negative (from the outside face) and positive (from the inside face of tubular pile) interface with the reduction factor (Rinter=0.5) to model an interaction roughness between the steel pile surface and clay soil in the case of the Al-Fao site, while assigned for a negative interface with the reduction factor (Rinter=0.7) to model an interaction roughness between the concrete pile surface and clay soil and assigned for a negative interface with the reduction factor (Rinter=0.8) to model an interaction roughness between the concrete pile surface and sandy soil.

Table 7. Interfaces for different materials [13]

Interaction Type	Interaction Factor (R_{inter})
Sand-Steel Interaction	0.6 - 0.7
Clay-Steel Interaction	0.5
Sand-Concrete Interaction	1.0 - 0.8
Clay-Concrete Interaction	1.0 - 0.7
Soil-Geogrid (grouted body)	1.0

2.7 Impact load modeling

The static and dynamic loads were modeled as a linear load of a circular shape for the tubular pile and as a point load at the center of the precast reinforced concrete piles. The static load values are the hammer weights listed in Table 5. The dynamic loads are modeled according to the waveforms of the hammers and the load multipliers shown in Figure 5. The load

multiplier is the factor multiplied by the specific load during impact time.

The load multiplier table allows you to define the time-dependent load variations for each load group and load stage. One way to depict changing loading circumstances is by using load multipliers that are specified as functions of time.

Once the load multiplier has been set and transferred to the Staged Construction dialog, proceed to assign the corresponding load groups to each load stage. This specifies the active loads for each phase of the simulation. After configuring the load groups, load stages, and load multipliers, proceed to execute the analysis. Plaxis 3D will calculate the behavior of the soil-structure system in response to the given dynamic loading conditions.

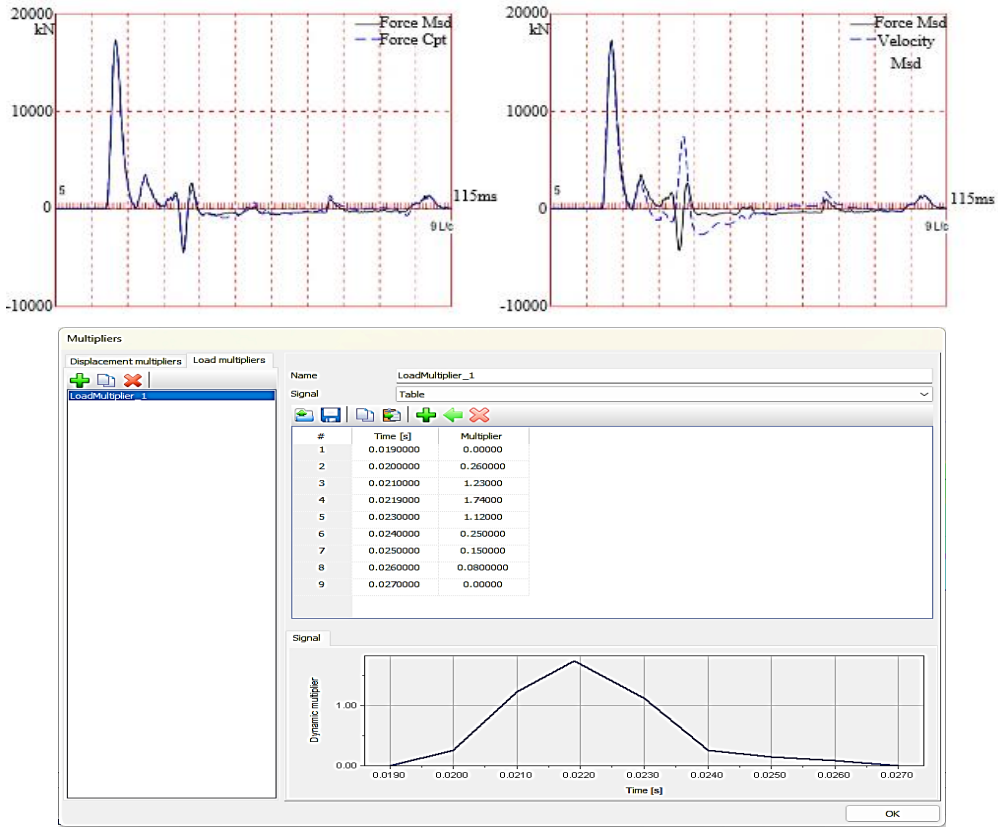

(A)

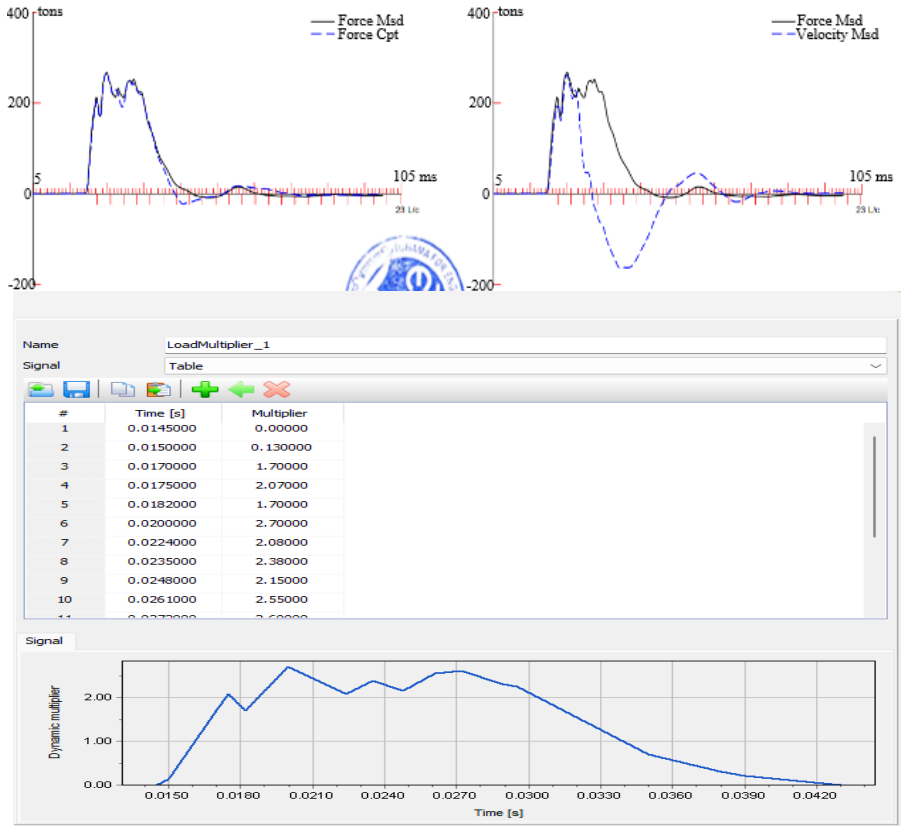

(B)

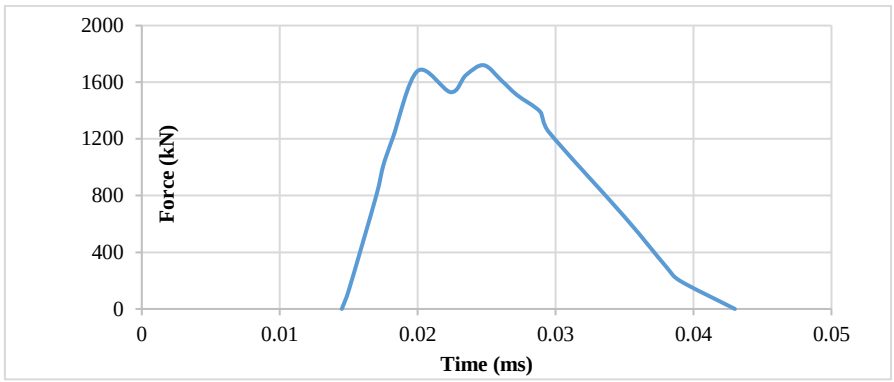

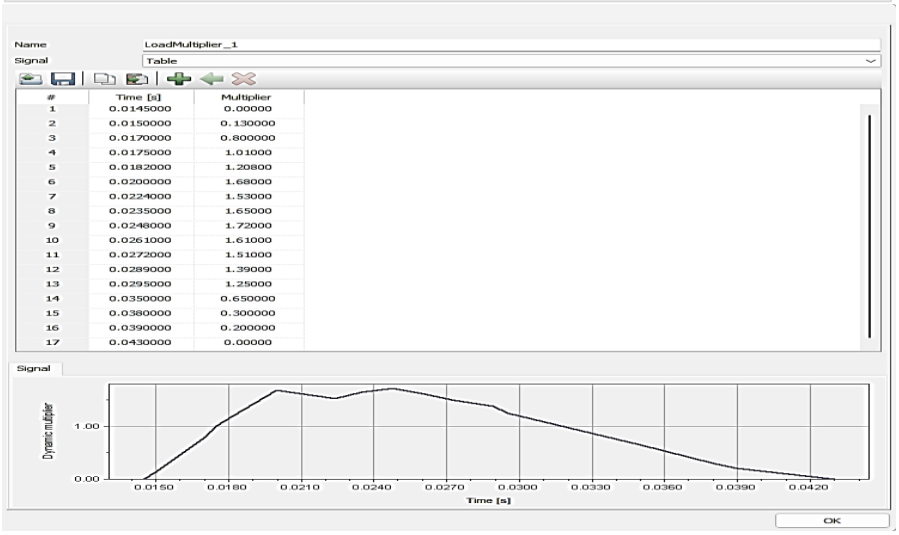

(C)

Figure 5. Dynamic load modeling of (A) Al-Fao site; (B) Shuaiba and (C) Umm qasr sites

2.8 Damping factor of the soil

Table 8. The damping factor of various types of soil [14]

Soil Type	Damping Factor
Clay	0.6 – 1.1
Silty Clay and Clayey Silt	0.4 – 0.7
Silt	0.2 – 0.45
Silty Sand and Sandy Silt	0.15 – 0.3
Sand	0.05 – 0.2

Table 9. Correlations between soil types and their properties [15]

Clayey Soil		
SPT	**Consistency**	**c_u (kPa)**
0 - 2	Very soft	< 12
2 - 4	Soft	12 - 25
4 - 8	Medium Stiff	25 - 50
8 - 15	Stiff	50 - 100
15 - 30	Very Stiff	100-200
> 30	Hard	> 200

Sandy Soil			
N-Value	**RD (%)**	**Packness**	**φ (deg)**
< 4	0-20	Very loose	< 30
4 - 10	20-40	loose	30 - 35
10 - 30	40-70	Medium dense	35 - 40
30 - 50	70-85	Dense	40 - 45
> 50	85-100	Very dense	> 45

Although the material damping is usually neglected in most cases, it is considered in this research. Table 8 lists the values of the damping factor (ξ) of various soil types. Within each type, the soil may be classified according to its stiffness or relative density (Table 9). The two tables are utilized in combination to determine the mean damping factors for the site soils. The assigned values are (1.02, 0.71, and 0.073) for Al-Fao, Shuaiba, and Umm Qasr sites.

2.9 Simulation phases

The simulation involved three distinct phases. The initial phase focuses on replicating the effective stress and pore water pressure within the soil. The second phase simulates both the elastoplastic drained and undrained analyses, taking into account the deformation of the soil caused by its weight, whereas pile driving and dynamic analysis are performed within the third phase.

3. RESULTS

The free vibration analyses are performed by removing pile hammer loads, to determine the natural frequencies. The results of forced vibration analyses are presented in terms of surface and body wave velocities (Figures 6-8). In addition to that, they are expressed as variations of (PPV) with distance from the vibration sources [16] for various pile penetrations (Figures 9-11).

The reduction in wave intensity (attenuation) occurs due to two factors: mainly on the wave propagation's geometry, known as geometric damping [1], and minorly the materials that the waves traverse, referred to as material damping [17].

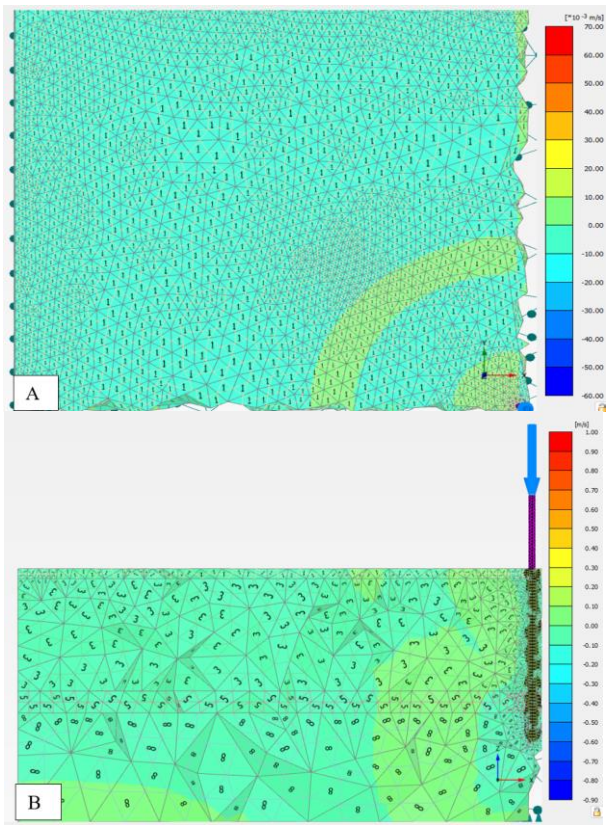

Figure 6. Wave velocities in Al-Fao site: (A) Surface wave; (B) Body wave

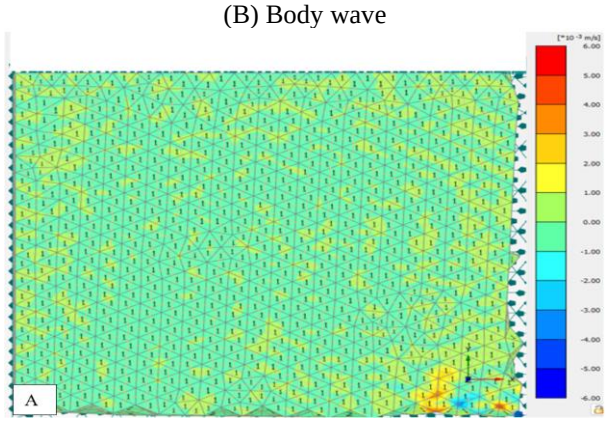

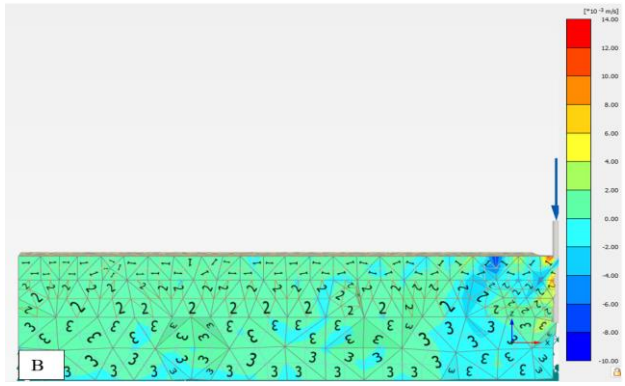

Figure 7. Wave velocities in Umm Qase site: (A) Surface wave; (B) Body wave

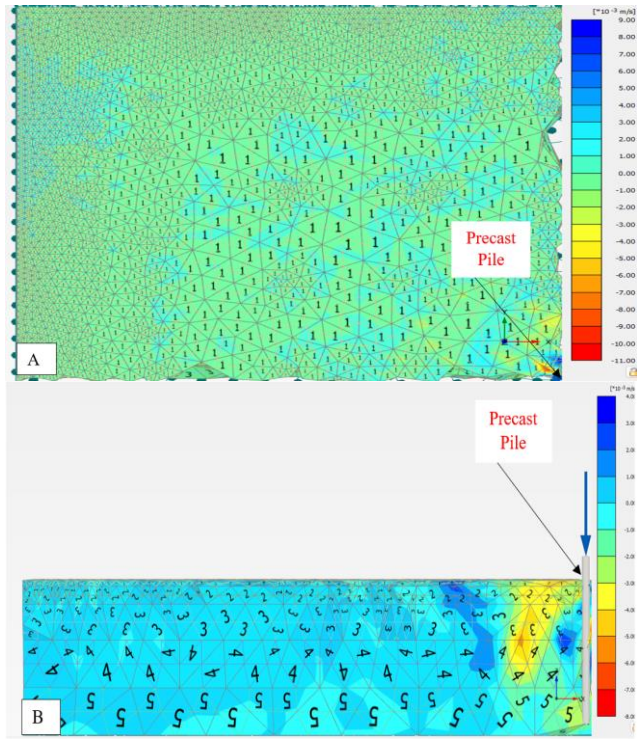

Figure 8. Wave velocities in Shuaiba site: (A) Surface wave; (B) Body wave

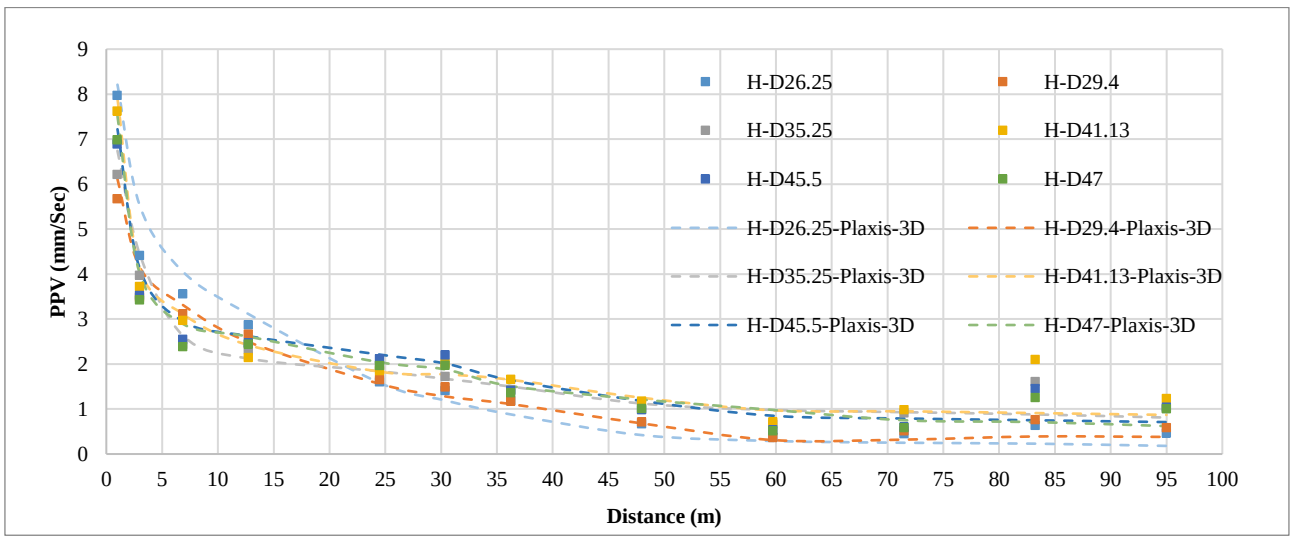

Figure 9. Predicted and measured PPV vs. distance for various pile penetrations (Al-Fao site)

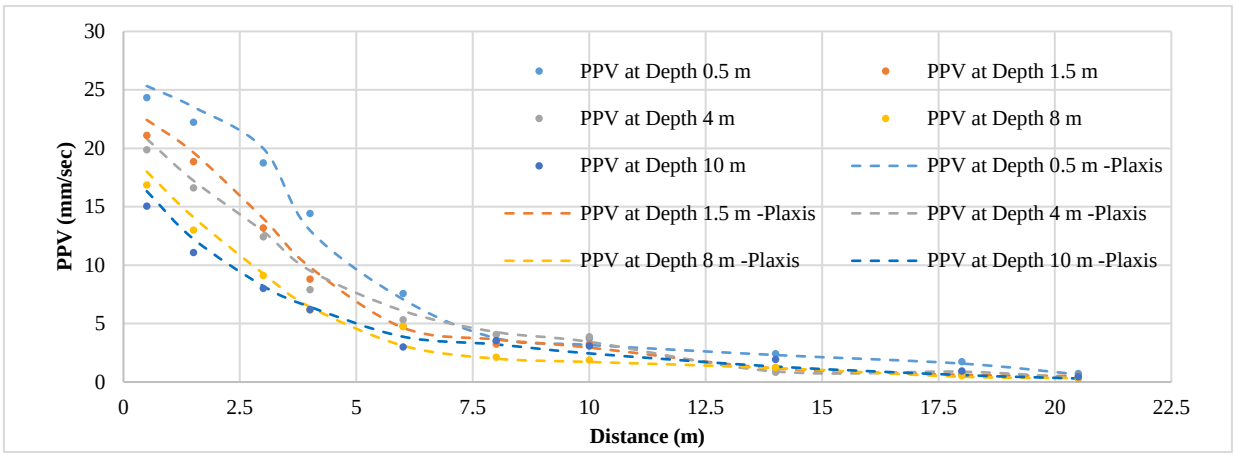

Figure 10. Predicted and measured PPV vs. distance for various pile penetrations (Shuaiba site)

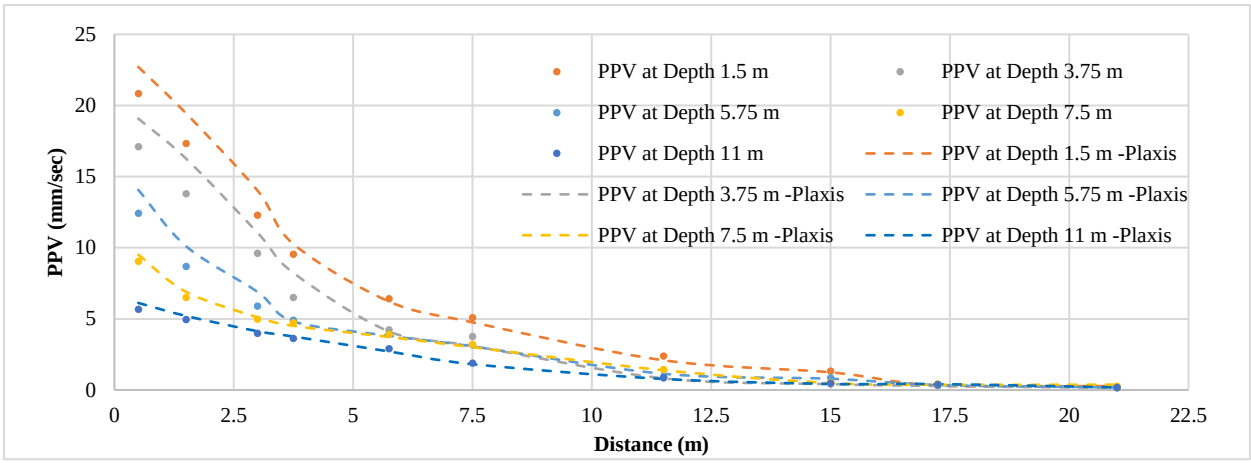

Figure 11. Predicted and measured PPV vs. distance for various pile penetrations (Umm Qaser site)

Table 10. Damping and absorption coefficients at the Al-Fao site

Depth (m)	r_1 (m)	r_2 (m)	Damping (A_2/A_1)
26.25	1	95	0.0577
29.4	1	95	0.1023
35.25	1	95	0.1626
41.13	1	95	0.1614
45.5	1	95	0.1509
47	1	95	0.1432

Table 11. Damping and absorption coefficients at the Shuaiba site

Depth (m)	r_1 (m)	r_2 (m)	Damping (A_2/A_1)
0.5	0.5	20.5	0.0259
1.5	0.5	20.5	0.023
4	0.5	20.5	0.0165
8	0.5	20.5	0.0186
10	0.5	20.5	0.0186

Table 12. Damping and absorption coefficients at the Umm Qaser site

Depth (m)	r_1 (m)	r_2 (m)	Damping (A_2/A_1)
1.5	0.5	21	0.1211
3.75	0.5	21	0.0079
5.75	0.5	21	0.0128
7.5	0.5	21	0.0395
11	0.5	21	0.0294

The rise in vibrations near the pile is mostly due to the direct effect of surface waves originating from the pile's surface. Conversely, the increase in vibrations at shallow depths, as opposed to deeper depths near the pile, is caused by the shorter travel of reflected waves from the pile's toe. This leads to a decrease in the reduction of energy as it passes through the soil (geometric damping) and the reduction of energy due to the soil's intrinsic properties (material damping) [14]. Due to the narrow wavelength in close proximity to the source, there is an elevation in the frequency of vibration. As the distance from the source rises, the amplitude of the vibration reduces, the length of the wave grows, and the frequency diminishes. The vibration strength and amplitude converge to a similar level when seen from a significant distance from the source. Based on the data provided in Tables 10-12, it can be shown that the Al-Fao model has the largest damping ratio (A_2/A_1) in comparison to the other models. The increased damping seen in the Al-Fao model may be ascribed to several variables. One of these aspects is the larger depth of the Al-Fao model compared to the other models. Additionally, the horizontal distances from the source also change between the Al-Fao model and the other models, making a direct comparison between them inappropriate owing to variances in circumstances. Furthermore, the Umm Qaser model exhibits substantial damping due to its comparable depths and horizontal distances to the Al-Shuaiba Model. Due to its lower hammer energy compared to other models, the Umm Qaser model exhibits a reduced dissipation of low-energy waves during propagation. Based on the data presented in Figures 6,

8, and 10, it is observed that the Al-Shuaiba model exhibits the highest values of PPV compared to the other models. This is because the Al-Fao model utilizes a tubular steel pile, which differs from the other models. Despite having the maximum hammer energy, the Al-Fao model has lower values of PPV due to the reflection and refraction of waves as they propagate through deeper depths. Additionally, the presence of surface waves has a negligible effect on the PPV compared to the presence of body waves. The Umm Qaser model, although having mostly sandy soil, has the same depths and distances as the Al-Shuaiba model. However, the Umm Qaser model has a greater capacity to transmit waves compared to Al-Shuaiba's soil. On the other hand, the hammer energy in the Umm Qaser model is lower than that of the Al-Shuaiba model.

Conclusively, it is difficult to undertake a thorough comparison of models, especially when taking into account the peak particle velocity (PPV). The challenge stems from the inherent differences in site circumstances, including changes in pile and hammer types as well as soil properties. Notwithstanding these difficulties, a comparison will be made between the models to clarify the influence of different pile and hammer types, as well as soil variables, on the measured PPV values:

(1) Soil conditions: According to Tables 1-3, the most common types of soil in Al-Fao were silty clay and clay in Al-Shuaiba whereas silty sand in Umm Qaser, the Al-Fao site has less attenuation due to the high depths and energy of the hammer which increase the body wave at a long distance while in Al-Shuaiba site has more attenuation due to the clay soil that tends to damp the vibration.

(2) Hammers: despite the hammer used in Al-Fao having the highest energy, the maximum PPV was detected in the Al-Shuaiba site which has a hammer's energy less than Al-Fao's Hammer, this is attributed to surface wave close to the pile in Al-Shiaiba was significant due the shallow depth as compared with Al-Fao Site.

(3) Piles: the pile used in Al-Fao was steel tubular that had the highest wave speed at the surface but due to the high pile impedance the induced vibration was less than the vibration in the Al-Shauiba site.

To evaluate the efficiency of the numerical simulation, regression analyses are performed between the predicted and measured (PPV) variations [18-20] with distance for various pile penetration depths. The results are listed in Table 13. A very good agreement is achieved.

Table 13. Results of regression analyses between the predicted and measured PPV

Site	R^2
Al-Fao	0.959
Shuaiba	0.986
Umm Qasr	0.975

Table 14. Maximum allowable PPV for transient vibrations to prevent structural damage [AASHTO 1990] [16]

Structure and Condition	Max. PPV mm/s
Engineered structures, without plaster	25.4 - 38.1
The residential building is in good repair with gypsum board walls.	10.16 - 12.7
Residential buildings, plastered walls	5.08 - 7.62
Historic sites or other critical locations	2.54

Many standards are available to provide the maximum permitted vibrations for various types of structures. In this study, the AASHTO standard will be used to determine the safe distance from pile driving (Table 14).

Referring to Figures 9 and 11 and Table 14, it can be realized that for a residential building with plastered walls, the safe distance is around 18 times the pile section dimension.

4. CONCLUSIONS

(1) The effectiveness of numerically simulating pile drive-produced vibrations using the finite element technique and Plaxis-3D software is evaluated. The regression analysis demonstrated a high level of agreement between the anticipated and measured behaviors.

(2) The presence of the impact hammer's waveform (as obtained from the PDA) is crucial for achieving an accurate simulation.

(3) Pile driving into a soil profile that includes a deep layer of soft soil has little impact on the shallow foundations of neighboring buildings.

(4) Typically, the recommended safe distance for regular residential structures is around 18 times the size of the pile section.

(5) The Al-Fao model has a very high level of damping, mostly attributed to its greater depths and longer horizontal measurement distances. In comparison, the Umm Qaser model shows a damping level that is twice as high as that of the Al-Shuaiba model.

(6) At the closest proximity to the piles, the Al-Shuaiba model recorded a maximum PPV value of 25.33 mm/s at a depth of 0.5 m. This value is three times higher than the PPV recorded by the Al-Fao model and 11.54% higher than the Umm Qaser model. These differences can be attributed to variations in the types of piles, hammers, depths, and horizontal distances.

(7) In both the Al-Fao model and the Umm Qaser model, the lowest PPV found was 0.18 mm/s. This occurred at a distance of 95m and 21m, and at a depth of 26.25m and 10m, respectively. In contrast, the Al-Shuaiba model had a lowest PPV of 0.304 mm/s at a distance of 21m and a depth of 11m.

ACKNOWLEDGMENT

I express my gratitude to GCPI Company for granting me access to the Daewoo Company site, where I obtained the necessary soil data. Additionally, I am thankful to Technital Company for their assistance with the same matter.

REFERENCES

[1] Woods, R.D. (1997). Dynamic effects of pile installations on adjacent structures (Vol. 7). Transportation Research Board.

[2] Nordal, S. (2009). Lecture notes: PhD course BA8305 Geodynamics. Norwegian University of Science and Technology, Trondheim, Norway.

[3] Massarsch, K.R., Fellenius, B.H. (2008). Ground Vibrations induced by impact pile driving. In Proceedings of the 6th International Conference on Case Histories in Geotechnical Engineering, Arlington.

[4] Zhang, M., Tao, M., Gautreau, G., Zhang, Z.D. (2013). A statistical approach to determining ground vibration monitoring distance during pile driving. Practice Periodical on Structural Design and Construction, 18(4): 196-204. https://doi.org/10.1061/(ASCE)SC.1943-5576.0000156
[5] Andersson Olivecrona, S., Sulander, R. (2016). Numerical analysis of vibrations due to impact pile driving. TVGT-5000.
[6] Grizi, A., Athanasopoulos-Zekkos, A., Woods, R.D. (2018). H-pile driving induced vibrations: Reduced-scale laboratory testing and numerical analysis. In IFCEE 2018, pp. 165-175. https://doi.org/10.1061/9780784481585.017
[7] Sun, Z., Yu, H., Li, C., Liu, R., Li, Q., Su, C. (2023). Ground and pile vibrations induced by pile driving. Buildings, 13(8): 1884. https://doi.org/10.3390/buildings13081884
[8] Tavasoli, O., Ghazavi, M. (2018). Wave propagation and ground vibrations due to non-uniform cross-sections piles driving. Computers and Geotechnics, 104: 13-21. https://doi.org/10.1016/j.compgeo.2018.08.010
[9] Hughes, T.J. (2012). The Finite Element Method: Linear Static and Dynamic Finite Element Analysis. Prentice Hall Englewood Cliffs, New Jersey.
[10] Geotechnical Interpretative Report of the Container Terminal in Al-Fao, Daewoo Company, Basra, AlFao.
[11] Soil Investigation Report of Shuaiba Refinery, Hyundai, Basra, Al-Shuaiba.
[12] Geotechnical Interpretative Report of Connecting Road in Umm Qaser. Daewoo Company, Basra, Umm Qasr.
[13] Brinkgreeve, R.B.J., Shen, R.F. (2011). Structural elements & modelling excavations in plaxis. Power Point Presentation File.
[14] Mihalache, A. (2016). Prediction of ground vibrations induced by impact driving of dolphin piles in Caland Canal. TU Delft Library.
[15] Terzaghi, K., Peck, R.B. (1948). Soil Mechanics in Engineering Practice. Wiley, New York.
[16] American Association of State Highway and Transportation Officials. (1990). Standard Recommended Practice for Evaluation of Transportation-Related Earthborne Vibrations. Washington, DC.
[17] Dowding, C.H. (1996). Construction Vibrations. Prentice-Hall, Upper Saddle River, USA.
[18] Saher, H.S., Al-Jubair, H.S., Ali, J.K. (2024). Measurements of induced vibrations due to steel pipe pile driving in Al-Fao soil: Effect of partial end closure. Open Engineering, 14(1): 20220550. https://doi.org/10.1515/eng-2022-0550
[19] Murali, D. (2016). Comparison of adaptive neuro-fuzzy based PSS and SSSC controllers for enhancing power system oscillation damping. Advances in Modelling and Analysis C, 71(1): 24-38.
[20] Laamari, Y., Allaoui, S., Bendaikha, A., Saad, S. (2021). Fault detection between stator windings turns of permanent magnet synchronous motor based on torque and stator-current analysis using FFT and discrete wavelet transform. Mathematical Modelling of Engineering Problems, 8(2): 315-322. https://doi.org/10.18280/mmep.080220

NOMENCLATURE

V_{H0}	Velocity of the hammer (m/s)
g	Acceleration due to gravity (m/s^2)
h	Height of drop (m)
$Z_{H,\,P}$	Hammer and pile impedance (kN.s/m), respectively
$V_{H,\,P}$	Hammer and pile particle velocity (m/s), respectively
L_p	Pile length (m)
C_p	The velocity of the wave in the pile (m/s)
$[M]$	Element mass matrix
$\{\ddot{d}\}$	Acceleration vector
$[C]$	Damping matrix
$\{\dot{d}\}$	Velocity vector
$[K]$	Element stiffness matrix
$\{d\}$	Displacement vector
$\{F\}$	Displacement vector
Vs	Shear wave velocity
E	Modulus of elasticity
γ	Density
υ	Poisson ratio
ζ	Damping factor